PARTICLE IMAGE VELOCIMETRY

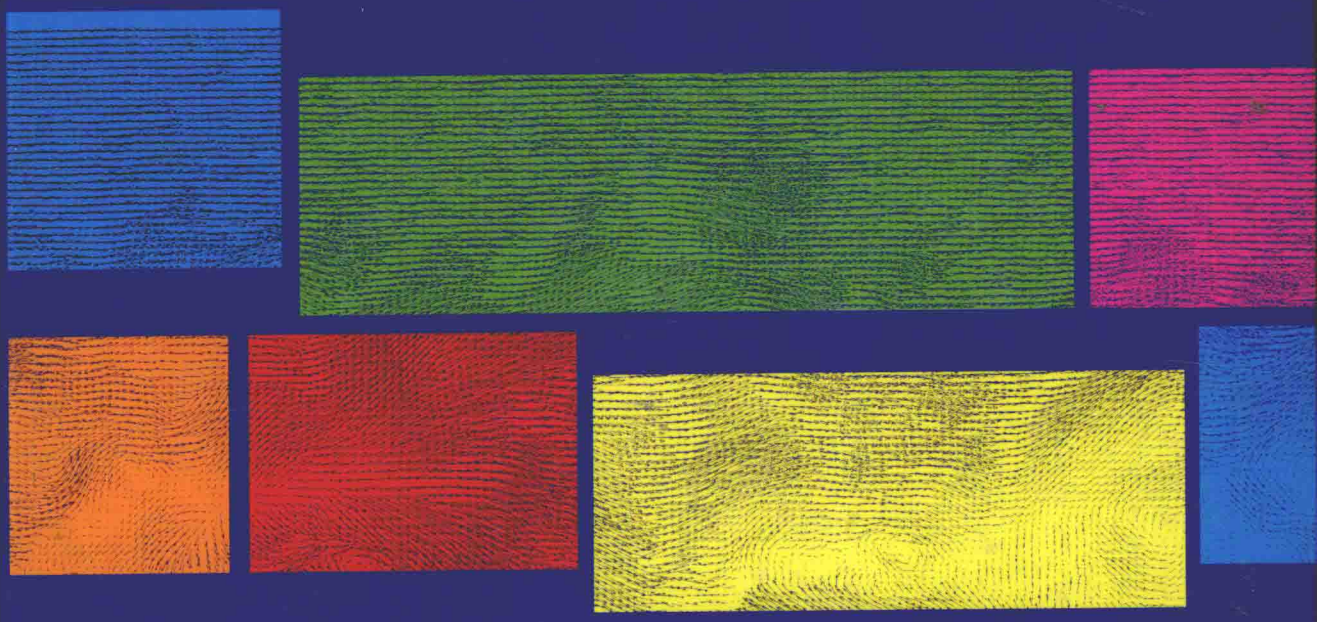

RONALD J. ADRIAN

JERRY WESTERWEEL

CAMBRIDGE

Particle Image Velocimetry

Ronald J. Adrian
Arizona State University

Jerry Westerweel
Delft University of Technology

CAMBRIDGE
UNIVERSITY PRESS

CAMBRIDGE UNIVERSITY PRESS
Cambridge, New York, Melbourne, Madrid, Cape Town, Singapore,
São Paulo, Delhi, Dubai, Tokyo, Mexico City

Cambridge University Press
32 Avenue of the Americas, New York, NY 10013-2473, USA

www.cambridge.org
Information on this title: www.cambridge.org/9780521440080

First published 2011

Printed in the United States of America

A catalog record for this publication is available from the British Library.

Library of Congress Cataloging in Publication data

Adrian, R. J. (Ronald J.), author.
Particle Image Velocimetry / Ronald Adrian, Jerry Westerweel.
p. cm. – (Cambridge Aerospace Series ; 30)
ISBN 978-0-521-44008-0 (hardback)
1. Particle image velocimetry. I. Westerweel, J. (Jerry), author. II. Title.
TA357.5.M43A37 2011
620.1′064–dc22 2010045675

ISBN 978-0-521-44008-0 Hardback

PARTICLE IMAGE VELOCIMETRY

Particle image velocimetry, or PIV, refers to a class of methods used in experimental fluid mechanics to determine instantaneous fields of the vector velocity by measuring the displacements of numerous fine particles that accurately follow the motion of the fluid. Although the concept of measuring particle displacements is simple in essence, the factors that need to be addressed to design and implement PIV systems that achieve reliable, accurate, and fast measurements and to interpret the results are surprisingly numerous. The aim of this book is to analyze and explain them comprehensively.

Ronald J. Adrian is the Ira A. Fulton Professor of Mechanical and Aerospace Engineering at Arizona State University. Dr. Adrian's research interests are the space–time structure of turbulent fluid motion and the development of techniques, both experimental and mathematical, to explore this structure. Techniques to which he has made fundamental contributions include laser-Doppler velocimetry, particle image velocimetry, and the optimal estimation method for analysis of turbulent flows. Dr. Adrian is a member of the United States National Academy of Engineering.

Jerry Westerweel is the fluid dynamics chair in the Laboratory for Aero en Hydrodynamics at the Delft University of Technology in the Netherlands. His research interests are turbulence and coherent flow structures, turbulent mixing and chemical reactions, disperse multiphase flows, microfluidics and biological flows, optical measurement techniques for quantitative measurements in flows such as particle image velocimetry, planar laser-induced fluorescence, and holography.

Cambridge Aerospace Series

Editors
Wei Shyy
and
Michael J. Rycroft

1. J. M. Rolfe and K. J. Staples (eds.): *Flight Simulation*
2. P. Berlin: *The Geostationary Applications Satellite*
3. M. J. T. Smith: *Aircraft Noise*
4. N. X. Vinh: *Flight Mechanics of High-Performance Aircraft*
5. W. A. Mair and D. L. Birdsall: *Aircraft Performance*
6. M. J. Abzug and E. E. Larrabee: *Airplane Stability and Control*
7. M. J. Sidi: *Spacecraft Dynamics and Control*
8. J. D. Anderson: *A History of Aerodynamics*
9. A. M. Cruise, J. A. Bowles, C. V. Goodall, and T. J. Patrick: *Principles of Space Instrument Design*
10. G. A. Khoury and J. D. Gillett (eds.): *Airship Technology*
11. J. Fielding: *Introduction to Aircraft Design*
12. J. G. Leishman: *Principles of Helicopter Aerodynamics*, 2nd Edition
13. J. Katz and A. Plotkin: *Low Speed Aerodynamics*, 2nd Edition
14. M. J. Abzug and E. E. Larrabee: *Airplane Stability and Control: A History of the Technologies that made Aviation Possible*, 2nd Edition
15. D. H. Hodges and G. A. Pierce: *Introduction to Structural Dynamics and Aeroelasticity*
16. W. Fehse: *Automatic Rendezvous and Docking of Spacecraft*
17. R. D. Flack: *Fundamentals of Jet Propulsion with Applications*
18. E. A. Baskharone: *Principles of Turbomachinery in Air-Breathing Engines*
19. D. D. Knight: *Numerical Methods for High-Speed Flows*
20. C. Wagner, T. Hüttl, and P. Sagaut (eds.): *Large-Eddy Simulation for Acoustics*
21. D. Joseph, T. Funada, and J. Wang: *Potential Flows of Viscous and Viscoelastic Fluids*
22. W. Shyy, Y. Lian, H. Liu, J. Tang, D. Viieru: *Aerodynamics of Low Reynolds Number Flyers*
23. J. H. Saleh: *Analyses for Durability and System Design Lifetime*
24. B. K. Donaldson: *Analysis of Aircraft Structures*, 2nd Edition
25. C. Segal: *The Scramjet Engine: Processes and Characteristics*
26. J. Doyle: *Guided Explorations of the Mechanics of Solids and Structures*
27. A. Kundu: *Aircraft Design*
28. M. Friswell, J. Penny, S. Garvey, A. Lees: *Fundamentals of Rotor Dynamics*
29. B. Conway (ed): *Spacecraft Trajectory Optimization*
30. R. J. Adrian and J. Westerweel: *Particle Image Velocimetry*

To our families,
who kept wondering when this book would be done.

Preface

Scope

This book is about particle image velocimetry, a fact that the reader can hardly escape, since it uses the acronym "PIV" roughly 1,300 times, more than twice per page. It was conceived in 1994, by which time the major elements of at least one "standard" version of the PIV instrument had been established. In this version a laser light sheet from dual pulsed lasers illuminated microspheres whose images were formed by a single lens and recorded as double exposures on photographic film using image shifting to extend the dynamic range. Many fundamental aspects of this technique were reasonably well understood, including the theory for two-dimensional image correlation, so it seemed a good time to summarize the subject in a book. However, a number of new ideas were entering the field – digital PIV, stereographic PIV, holographic PIV, advanced image processing and extended methods of PIV analysis, to name a few – so there was an equally good argument for delaying the book until these ideas were more developed. In the end, the pace of new ideas, like micro-PIV, tomographic PIV, and self-calibration, and the time needed to evaluate them delayed writing until the last few years. This is not to say that activity in the area of PIV has slowed; only that we could not wait any longer.

The intent of this book is to provide a description of the PIV technique that is unified, is reasonably complete as of the time of writing, and provides the reader with easy access to the tools needed to understand various aspects of PIV: optics and image formation, light scattering by particles, particle dynamics, digital image recording and analysis, speckle, and analysis of random signals, including random vector fields as they relate to flow visualization. Its principal goal is to enable the reader to perform high-quality measurements with PIV. The intended audience is anyone who wants to use PIV to perform experiments: students, researchers, and practicing professionals in science and engineering.

We have endeavored to make this book useful to all levels of experience from first-time users of PIV through to experts. One can, of course, read the chapters in order from beginning to end. But, in order to enable the first-time user to operate a PIV system as soon as possible, Chapter 1 is designed to introduce all of the essential aspects of a complete PIV system and to perform a PIV experiment using an existing single-camera system. It can, for example, be used for introducing PIV in a teaching laboratory. The description of PIV systems in Chapter 5 presents the array of capabilities that are possible beyond those of the single-camera

system. It can be used by the first-time user to select the type of system that is needed, or by the advanced user to understand details of the various techniques. Lastly, Chapter 10 describes many techniques and practices for optimizing the PIV measurements to achieve the highest-quality data in practice. This knowledge is often hard won in practice, and we hope that it will provide the new user with a fast path to highly successful experiments. In summary, the beginner should read only Chapters 1, 5, and 10.

Chapters 2, 3, and 4 and Appendices 1 and 2, describe particle technology, optics, and digital imaging and digital Fourier transforms as they pertain to PIV. Some knowledge of each of these subjects is needed in reading Chapters 1, 5, and 10, so the reader may find it necessary to refer to these chapters. They can also be used to teach optics, imaging principles for flow visualization, digital image processing, and digital cameras in a course on experimental mechanics.

Chapters 6, 7, and 8 contain the theory of PIV and the development of many of the practical operating rules from first principles. These treatments give deep understanding of the PIV methods and provide the bases for understanding future developments.

Throughout the book we have attempted to introduce various concepts and methods, first by describing a simple rule-of-thumb, then explaining how this rule was found or defined, and finally presenting an underlying theoretical analysis, optimization, or simulation. So, a novice user will find a quick answer, while more advanced users may continue to read and discover the origin of certain practices. At the deepest level the reader may find a basis for further research and improvement of the PIV method.

One of the most important contributions of PIV to experimental fluid dynamics is its capability to measure instantaneous velocity fields. Such fields can be analyzed by various methods discussed in Chapter 9. These methods provide more refined descriptions of the kinematics of fluid flow.

Acknowledgments

The community of researchers who worked on the early development of PIV shared its knowledge generously, and the list of references only begins to acknowledge their many contributions. A few in particular have been especially influential colleagues: Dan Bjorkquist, Mory Gharib, Klaus Hinsch, Jürgen Kompenhans, W. Lai, Zi-Chao Liu, Fulvio Scarano, Bernd Wieneke, and Chris Willert. JW is thankful to the late Frans Nieuwstadt who convinced him to contribute to this book.

We also wish to acknowledge the many important contributions over the years from research students, postdoctoral students, and visiting scholars to our laboratories. This work would not exist without their insights and dedication.

Many thanks are due to Donald Rockwell, Michele Milano, B. J. Balakumar, Durella O'Donnell, Christian Poelma, and Ken Kiger for reading and commenting on drafts of this book. Their thoughts always led to improvements.

We are grateful to the Leonard C. and Mary Lou Hoeft Endowment at the University of Illinois, Urbana-Champaign; the Ira A. Fulton Endowment for Engineering at Arizona State University; and the many funding organizations and companies that supported the research of the authors into the theory and development of PIV over almost thirty years. Special thanks to the Burgers Program of the University of Maryland, which hosted JW to write significant parts of this book during his 2007 sabbatical.

Lastly, and most importantly, we thank our families for their support and understanding.

Ronald J. Adrian, Tempe, 2010
Jerry Westerweel, Delft, 2010

Nomenclature

Roman symbols

A, A_I	area of interrogation domain (m^2)	19
A, B	complex scattering coefficients	(2.45)
A($\boldsymbol{X}$)	total complex amplitude ($W^{1/2}/m$)	(3.51)
$\boldsymbol{A}$, $\boldsymbol{B}$	calibration coordinate matrices (m)	(3.16)
$A_{m,n,p,q}$	image transformation matrix	(4.27)
A_{ij}	velocity gradient tensor (s^{-1})	(9.64)
a	local variation of the displacement (m)	(8.109)
$\boldsymbol{a}$, $\boldsymbol{a}'$, $\boldsymbol{b}$, $\boldsymbol{b}'$	algebraic mapping coefficients	(3.11)
a_m	mode amplitude (m/s)	(9.92)
a_k	image complex amplitude per unit illumination amplitude of kth particle	105
B	background intensity or gray level	(7.29)
$\mathbb{B}(k, n; p)$	binomial distribution	(2.59)
$\boldsymbol{b}$	particle body force per unit mass (m/s^2)	14
$\boldsymbol{b}$	bias error of measured velocity (m/s)	(9.22)
C	tracer number density (m^{-3})	12
C_1, C_2	cost function weight constants	(6.11)
$C_{i,j}$	correspondence in cluster correlation	(7.51)
$C_{i,j}$	binary correlation	(8.183)
C_{ki}	velocity correlation between frames i and k	(9.122)
c_τ	uncertainty in particle image location relative to d_τ	34
c_ϕ	normalization constant for wavelet transform	481
c_m	Fourier mode coefficient (m/s)	(9.100)
D	diameter of pipe or cylinder (m)	Figure 10.8
$\mathbb{D}$	(particle) diffusivity (m^2/s)	70
D_I	linear dimension of interrogation area (m)	26
D_0	peak detectability	(8.77)
D_a	diameter of lens aperture (m)	9
d_a	diameter of aberrated image of a point source (m)	9
d_D	width of the displacement-correlation peak (m)	(8.126)

d_Δ	width of the displacement distribution within $W(\boldsymbol{X})$ for uniaxial strain (m)	Figure 8.36
d_f	fringe spacing (m)	(3.137)
d_I	D_I / M_0 (m)	22
d_p	particle diameter (m)	8
d_r	pixel pitch (m)	16
d_s	diffraction-limited spot diameter (m)	(1.7)
d_z	geometric particle image diameter of point-like object as a function z (m)	(3.34)
d_τ	particle image diameter (m)	8
E	event	467
$\mathcal{E}$,$\mathcal{E}_p$	exposure, for particle p (J/m^2)	16,(1.15)
E	complex amplitude of light wave (W$^{1/2}$/m)	(2.42)
E_1, E_2	errors of the first and second kind, respectively	(6.10)
$\bar{\mathcal{E}}_p$	mean exposure for pth particle (J)	(3.126)
$E(z)$	(complex) amplitude of the light sheet intensity $\mathcal{J}(z)$	(8.61)
$\boldsymbol{e}, e_i$	eigenvector	(9.66)
e	mode sum error	(9.101)
$\mathcal{F}$	Fourier transform operator	27
$\mathsf{F}(\chi, \psi)$	Fourier transform of the optical point-spread function	(7.16)
$\boldsymbol{F}(\boldsymbol{x})$	image mapping function of point $\boldsymbol{x}$ in object space (m)	10
$\hat{\boldsymbol{F}}(\boldsymbol{x})$	approximate algebraic form of mapping function (m)	90
$\boldsymbol{F}$	force acting on particle or object (N)	(2.1)
F_I	in-plane loss of correlation	25
F_O	out-of-plane loss of correlation	(1.31)
F_Δ	loss of correlation due to local gradients	(2.78)
$F_\tau(\boldsymbol{s})$	particle image self-correlation (m^{-2})	(3.74)
f	lens focal length (m)	7
f_o	objective lens focal length (m)	Figure 5.48
$f^\#$	lens aperture number	(1.8)
$f^\#_\infty$	infinity-corrected aperture number	(5.17)
$f(\boldsymbol{x}', t'; \boldsymbol{x}, t \mid \boldsymbol{u})$	conditional transition probability (m^{-3})	69
f	filter length (m)	Figure 6.5
f_0	$1/2\pi\tau_0$ (s^{-1})	(2.33)
f_o, f_b	probability density functions of object and background pixels, respectively	(6.12)
f_s, f_n	probability density functions of the signal peak and tallest noise peak in the correlation	(8.81)
f_H	factor	(2.13)
$f(\boldsymbol{w}\mid\boldsymbol{\theta})$	joint probability density function of $\boldsymbol{w}$ for given $\boldsymbol{\theta}$	(7.36)
$G(X, Y)$	paraxial projection of $g(\boldsymbol{x}, t)$ (m^{-2})	(3.60)
$\mathcal{G}(X, Y)$	projection of $g(\boldsymbol{x}, t)$ for Young's fringe analysis	(8.62)
$\mathsf{G}(\chi, \psi)$	Fourier transform of pixelized particle image	(7.11)

$\mathsf{G}(\boldsymbol{x})$	spatial correlation of $\mathsf{E}(\boldsymbol{X})$	(8.57)
$\boldsymbol{g}$	gravitational acceleration (m/s^2)	40
g_B	background gray-level noise	139
$\mathrm{g}(i, j)$	gray level	(3.134)
g'_n	fluctuating component of the pixel noise	(3.138)
$g(\boldsymbol{x}, t)$	particle indicator function (m^{-3})	(1.19)
$g(X, Y; \boldsymbol{\theta})$	parameterized model for $\tau(X, Y)$	290
H	filter length for Gaussian data interpolation	(9.7)
H_I, H_O	equivalents of F_I and F_O for Young's fringe analysis	(8.71)
$H(i, j)$	image transform representation	(4.27)
$\mathsf{H}_p(\omega)$	complex particle frequency response function	(2.21)
$\mathcal{H}(\boldsymbol{s})$	optical transfer function	98
$\mathcal{H}(t)$	Heaviside step function	48
$H(X, Y)$	Gaussian model for $\tau(X, Y)$ integrated over pixel area	(7.26)
h	distance from optical axis (m)	Figure 3.3
h	Planck's constant (J s)	134
$h(X, Y; \boldsymbol{\theta})$	parameterized model for $\tau(X, Y)$	285
$\mathsf{h}(\boldsymbol{s})$	Fourier transform of $\lvert\mathsf{P}\rvert^2$	97
$I(X, Y)$	light intensity in image plane (W/m^2)	(1.18)
I^*	normalized image intensity	(3.115)
$I_o(\boldsymbol{x})$, $I_i(\boldsymbol{X})$	light intensity in the object plane and image plane (W/m^2)	98
$I_g(\boldsymbol{X})$	geometrical optics image intensity (W/m^2)	(3.27)
$\bar{I}_N$	speckle noise intensity (W/m^2)	235
$I_p(\boldsymbol{X})$	image intensity of particle p (W/m^2)	103
$I(i, j)$	discretized image intensity (W)	(1.25)
$I^\bullet$	intensity equivalent to image gray value (W/m^2)	151
I_θ	gray-level threshold value for image segmentation	Figure 6.2
$\mathcal{J}(z)$	illuminating beam intensity (W/m^2)	10
$\mathcal{J}_0$	maximum value of $\mathcal{J}(z)$ (W/m^2)	105
J_A	mutual intensity	(3.54)
J_α	mutual density at exit pupil	(3.56)
J	light energy flux (W/m^2)	(2.53)
J_0	total energy in light pulse (J)	10
$J_0(s)$, $J_1(s)$	zeroth- and first-order Bessel functions of the first kind	73
K	cost function	(6.11)
$\mathbb{K}$	proportionality constant between intensity and gray level	(3.135)
$K(t)$	memory kernel for Basset history force	(2.12)
$\mathsf{K}(z)$	reconstruction kernel for digital holography	(3.149)
K_4	fourth-order correlation term	(8.175)
$\boldsymbol{k} = (k_x, k_y, k_z)$	wave number (m^{-1})	27
k_B	Boltzmann's constant (J/K)	70
L	half-width of interrogation domain (m)	72
L_{ij}	coefficient of linear stochastic estimate	(9.86)

L_X, L_Y	linear dimensions of the recording medium (m)	35
L_x, L_y	in-plane linear dimensions of the measurement volume (m)	302
$\mathcal{L}$	linear integral scale of spatial correlation	(4.26)
ℓ	length, length scale (m)	
ℓ_X, ℓ_Y	linear dimensions of field of view in fluid (m)	(1.68)
M, N	number of pixels per column and row, respectively	22
$\mathbb{M}$	minimum variance bound	(7.38)
M_0	nominal or paraxial image magnification	7
m	ratio of refractive indices n_p and n_f	(2.46)
$\boldsymbol{m}_D$	centroid of the instantaneous correlation peak	(8.106)
m_p	particle mass (kg)	(2.9)
N	number of particles in interrogation spot	25
$\mathcal{N}$	number of particles in flow field	66
N_F	number of image frames	Figure 9.16
N_I	image density	(1.28)
N_K	number of data points per row	Figure 9.16
N_M	number of dye molecules in particles	58
N_P	number of superimposed correlations	8.87
N_R	mean number of successful measurements per unit area (m^{-2})	(8.191)
N_S	source density	(1.21)
N_c	number of calibration points	94
N_e	mean number of electrons in CCD well	(3.132)
NA	numerical aperture	207
$\mathbb{N}(\mu, \sigma^2)$	normal distribution	348
$\boldsymbol{n}$	normal vector	(1.58)
n	number of particles in interrogation volume	(2.56)
n_f	fluid refractive index	15
n_p (n_p)	(complex) refractive index of particle	51
OD	optical density	(3.130)
P	probability that particle image overlaps with another	(7.1)
P	(complex) pupil function of imaging lens	(3.24)
$P(\chi, \psi)$	Fourier transform of $p(X, Y)$	(7.11)
P_0	interrogation success rate	Table 7.2
P_C	particle image detection probability (for thresholding)	(8.190)
$P_{\max}$	maximum probability for successful particle image match	(7.63)
$\mathcal{P}$, $\mathcal{Q}$, $\mathcal{R}$	scalar invariants of $\partial u_i/\partial x_j$	(9.68)
p	pressure (Pa)	32
$\hat{\boldsymbol{p}}$	polarization unit vector	50
$p(\boldsymbol{X})$	pixel sensitivity (m^{-2})	16
p_{RI}	random phasor sum probability density function	(3.52)
$\mathcal{Q}$	volume flux (m^3/s)	(1.62)
Q_{ij}	two-point velocity correlation tensor (m^2/s^2)	(1.63)
q	difference between image quantization levels	(4.14)

$\boldsymbol{Q}$	velocity correlation tensor (m^2/s^2)	(1.63)
$R(\boldsymbol{s})$	spatial correlation (J^2/m^2)	(1.35)
$R^*(\boldsymbol{s})$	single-pixel correlation	(8.52)
$R^*(\boldsymbol{s})$	unbiased estimator for the spatial correlation	(8.104)
R_C	correlation of mean image intensity in interrogation domain	(8.5)
R_D, R_{D^+}, R_{D^-}	displacement-correlation peak (J^2/m^2)	25
$\langle R_D \vert \boldsymbol{u} \rangle$	ensemble mean of R_D over all possible particle image patterns for given $\boldsymbol{u}$	(8.15)
R_F	correlation of image fluctuations and mean image intensity	(8.6)
R_P	self-correlation peak (J^2/m^2)	25
Ra_0,Ra_1	Rayleigh length of laser beam (m)	(5.1)
Re	Reynolds number	14
r	absolute deviation, or residual, of displacement from neighboring values (m)	(9.1)
$\boldsymbol{r}$	scattering direction vector (m)	Figure 2.4
r_{ij}	rotation tensor (s^{-1})	31
$S(\chi, \psi)$	image power spectral density	148
S_C, S_P	optical Fourier transforms of $\langle \mathsf{G}_C \rangle$ and $\langle \mathsf{G}_P \rangle$, respectively	(8.76)
$\boldsymbol{s}$	position vector in the correlation plane (m)	23
$\boldsymbol{s}_0$	most likely particle image displacement (m)	(8.142)
$\boldsymbol{s}_D$	position of the displacement-correlation peak (m)	(3.71)
$s_{D,X}$, $s_{D,Y}$	components of $\boldsymbol{s}_D$	(8.102)
s_{ij}	strain rate tensor (s^{-1})	(1.54)
s_m	median displacement vector (m)	(9.1)
s_Δ	centroid of the displacement distribution within $W(\boldsymbol{X})$ for uniaxial strain (m)	Figure 8.36
T	(absolute) temperature (K)	70
$\mathcal{T}$	time interval (for time average) (s)	(9.26)
$\mathsf{T}(\chi, \psi)$	Fourier transform of $\tau(X, Y)$	280
t	time (s)	8
t	complex transmissivity (including phase change)	(8.53)
t^*	$t + \frac{1}{2}\Delta t$	30
Δt	exposure time delay (s)	8
δt	duration of the illumination pulse (s)	16
δt_e	min{duration of laser pulse, duration of shutter time} (s)	(3.124)
$\mathsf{U}(X, Y)$	complex light amplitude in image plane	97
$\mathsf{U}_p(\boldsymbol{X})$	complex light amplitude of pth particle	105
U_n, V_n	Lommel functions	(3.19)
U_0	material velocity behind a passing shock wave (m/s)	48
$\boldsymbol{u}(\boldsymbol{x}, t)$	velocity field (m/s)	27
Δu	local variation of the velocity (m/s)	(9.31)
$\hat{\mathsf{u}}$	complex amplitude of Fourier transform of velocity (m)	45

$\boldsymbol{u}_0$	measured velocity for finite interrogation domain	(8.89)
$\tilde{\boldsymbol{u}}$	measured velocity (m/s)	(9.22)
$\tilde{u}, \tilde{v}$	spatially filtered velocity data	(9.4)
V	(measurement) volume (m^3)	12
$\boldsymbol{V}$	set of proper orthogonal decomposition eigenvectors	(9.124)
V_t	instantaneous equivalent volume that corresponds to interrogation area	(7.53)
V_{in}	fluid volume that is swept into V_t during exposure	(7.53)
$\mathbb{V}$	covariance matrix	(7.41)
$\boldsymbol{v}, \boldsymbol{v}_p$	velocity of (pth) tracer particle (m/s)	29
$\mathcal{V}$	total flow volume	
v_{px}, v_{py}	in-plane velocity components of $\boldsymbol{v}_p$ (m/s)	(1.4)
$\dot{\boldsymbol{v}}_p$	particle acceleration (m/s^2)	(1.22)
$\ddot{\boldsymbol{v}}_p$	particle jerk (m/s^3)	31
$\hat{\mathsf{v}}_p$	complex amplitude of particle frequency response (m)	45
W	image window function	23
$W(W_P)$	(Parzen) image band width (m^{-1})	148
W	total illumination energy (W)	129
W_α	$\exp(-2\pi \mathrm{i}/\alpha)$	(4.28)
$\mathcal{W}(\boldsymbol{X})$	weight function for velocity field $\boldsymbol{u}(\boldsymbol{x}, t)$ representing finite interrogation domain	(1.41)
w	out-of-plane component of the velocity (m/s)	20
w	maximum path length error (m)	(3.29)
w_0, w_1	beam waist (m)	(5.1)
$\boldsymbol{X}$	position vector in image domain (m)	6
$\boldsymbol{X}_{ij}$	position vector of pixel with indices (i, j)	16
X,Y	in-plane coordinates of $\boldsymbol{X}$ (m)	6
$\Delta\boldsymbol{X}$	displacement vector in image domain (m)	8
$\boldsymbol{X}_I, \boldsymbol{x}_I$	interrogation location in image plane and object space, respectively (m)	18
$\boldsymbol{X}_L, \boldsymbol{X}_R$	image positions for left and right camera in stereoscopic viewing	35
$\Delta\boldsymbol{X}_M$	mean particle-image displacement (m)	Figure 8.71
$\boldsymbol{X}_p(t)$	position of image of pth particle as a function of time t (m)	7
$\boldsymbol{X}_s$	image shift (m)	Figure 8.9
$\boldsymbol{Z}_x, \Delta\boldsymbol{x}_p$	particle displacement (m)	8
$\Delta\boldsymbol{X}_p$	particle image displacement of particle p (m)	8
$\langle\widetilde{\Delta X}\rangle$	mean measured displacement	(7.67)
$\boldsymbol{x}$	position vector in flow domain (m)	6
x,y	in-plane coordinates of $\boldsymbol{x}$ (m)	6
$\boldsymbol{x}_C$	critical point in flow field	460
$\boldsymbol{x}_c$	coordinate of calibration point (m)	94
$\boldsymbol{x}_p(t)$	position of pth particle as a function of time t (m)	30

$\bar{\boldsymbol{x}}_p$	midpoint of $\boldsymbol{x}_p(t)$ and $\boldsymbol{x}_p(t+\Delta t)$	(1.48)
$\delta x, \delta y$	data spacing (m)	27
Δy_0	height of the light sheet (m)	11
Z	out-of-plane coordinate of $\boldsymbol{X}$ (m)	Figure 1.3
z	out-of-plane coordinate of $\boldsymbol{x}$ (m)	Figure 1.3
Z_0, z_0	image distance and object distance (m)	7
z^*	offset distance between light sheets (m)	Figure 5.24
z_P	evanescent wave penetration depth (m)	(5.19)
Δz	out-of-plane displacement (m)	Figure 1.15
Δz_0	thickness of the light sheet (also $\Delta z_0'$ and $\Delta z_0''$) (m)	7
δz	depth of field (m)	(1.9)

Greek symbols

α	tilt angle of the image plane (rad)	Figure 1.15
α	reliability level of interrogation result	Figure 7.22
α	absorption coefficient for a fluorescent dye	58
α	dimensionless particle size ($=\pi d_p/\lambda$)	(2.47)
α_k	$=\lvert \mathsf{a}_k \rvert$	Figure 3.22
α_k	weight factor for data interpolation	(9.7)
α_p	$=\sqrt{\mathcal{J}(z_p)}a_p(X, Y)$ ($\mathrm{W}^{1/2}$/m)	(3.51)
α_1	probability that no other particle images occur within distance R_1	(7.75)
β^2	parameter in Gaussian approximation	(3.32)
β^2	pixel fill factor	148
β	quality factor for holographic reconstruction	235
Γ	circulation (m^2/s)	(1.58)
Γ	valid detection probability	Table 9.1
γ	(local) shear rate (s^{-1})	72
γ	power-law coefficient for nonlinear film optical density	(3.131)
γ	ratio of random error variance and velocity variance	(9.59)
Δ	discriminant of polynomial	465
$\Delta_{i,j}$	digital mask	(8.189)
δ_0	mean distance between particle images (m)	278
$\delta_{\Delta X}$	error in the measurement of ΔX (m)	413
$\delta(s)$	Dirac δ-function	66
δ_{ij}	Kronecker δ-symbol	445
δz_c	correlation depth (m)	(8.137)
ϵ_X	(random) error in estimated particle image location (m)	(7.13)
ϵ	turbulence dissipation rate (per unit mass) ($\mathrm{m}^2/\mathrm{s}^3$)	(9.25)
ε	Stokes number	(2.23)
ε	dye emissivity	58
ε	threshold value for correlation depth	(8.137)
$\hat{\varepsilon}$	subpixel displacement interpolator	(8.161)

ε_B	random error amplitude owing to Brownian motion	(5.18)
$\varepsilon_X, \varepsilon_Y$	relative perspective error in in-plane displacement	(3.7)
Φ_{pp}	pixel sensitivity self-correlation (m^{-2})	(4.22)
ϕ	correction function for particle dynamics	14
ϕ	angle of optical ray with optical axis (rad)	Figure 3.3
ϕ	laser beam divergence (rad)	(5.2)
ϕ, ψ	dimensionless coordinates	96
$\phi_k(\boldsymbol{X})$	phase of complex image amplitude of kth particle (rad)	105
$\phi_m(y)$	basic mode for decomposition	(9.92)
$\phi(s)$	wavelet kernel	(9.129)
$\varphi_m(y)$	Fourier mode	472
κ_4	fourth cumulant of intensity fluctuations	(8.176)
$\Lambda(s)$	triangle function	Figure 4.4
λ (λ_0)	light wavelength (in vacuum) (m)	9
λ_K, λ_T	Kolmogorov and Taylor length scales, respectively (m)	(9.24)
$\boldsymbol{\mu}, \boldsymbol{\mu}_D$	centroid of particle image or correlation peak (m)	(7.2)
$\boldsymbol{v}_\mathrm{r}, \boldsymbol{v}_\mathrm{cr}, \boldsymbol{v}_\mathrm{ci}$	eigenvectors for complex eigenvalues of A_{ij}	Figure 9.28
ρ_f	fluid density (kg/m^3)	14
ρ_p	tracer density (kg/m^3)	14
$\bar{\rho}$	ratio of particle density and fluid density	(2.16)
$\varrho(k)$	correlation coefficient of measured velocity fluctuations	(9.33)
τ	transmissivity of optical film	131
τ	(wall) shear stress (Pa)	(9.19)
$\tau(\boldsymbol{X})$	image intensity in interrogation window (J/m^2)	(8.2)
$\tau(i, j)$	pixelized version of $\tau(\boldsymbol{X})$ (J/m^2)	(7.23)
$\tau_0(\boldsymbol{X})$	(mean) exposure of a particle image per unit of illuminating beam intensity	10
τ_0	low-pass-filter time constant	(2.32)
$\tau_0(\boldsymbol{X})$	mean particle image intensity particle per unit of illumination intensity	104
τ_{00}	total particle image intensity per unit illumination (m^2)	(3.62)
τ_p	particle response time constant (s)	(1.23)
$\tau_p(\boldsymbol{X})$	image intensity of pth particle per unit of illumination intensity	103
$\boldsymbol{\sigma}$	scattering coefficient ($rad^{1/2}/m$)	51
$\lvert\sigma\rvert^2$	light scattering cross section of a particle (m^2/srad)	11
σ^2	random phasor variance	(3.53)
σ^2	constraint cost function in optical flow optimization	(8.188)
$\sigma^2_{\mathrm{g,SN}}$	mean square shot noise	(3.137)
σ_I^2	variance of intensity fluctuations	(8.176)